Piezoelectric effect and diode effect in anapole and monopole superconductors

Michiya Chazono ◉,[*] Shota Kanasugi ◉, Taisei Kitamura ◉, and Youichi Yanase
Department of Physics, Kyoto University, Kyoto 606-8502, Japan

Superconductors lacking both inversion symmetry and time-reversal symmetry have been attracting much attention as a platform for exotic superconducting phases and anomalous phenomena, including the superconducting diode effect. Recent studies revealed intrinsic phases with this symmetry, named anapole superconductivity and monopole superconductivity, which are PT-symmetric superconducting states with and without Cooper pairs' total momentum, respectively. To explore characteristic phenomena in these states, we calculate and predict the superconducting piezoelectric effect and superconducting diode effect. A close relationship with the finite-q pairing, asymmetric Bogoliubov spectrum, and quantum geometry is discussed. This study reveals the piezoelectric and diode effects as potential probes to elucidate exotic superconducting phases.

I. INTRODUCTION

In recent years, superconductors lacking both inversion symmetry (IS) and time-reversal symmetry (TRS) have received much attention. For instance, nonreciprocal charge responses are extensively studied in superconductors with such symmetry [1–9]. In particular, the superconducting diode effect has become a central topic in condensed matter physics, and vast experimental and theoretical studies are conducted [10–26]. These nonreciprocal phenomena are expected to be ubiquitous since the simultaneous breaking of IS and TRS can be realized in various situations. Superconductors with noncentrosymmetric crystal structures under magnetic fields are typical examples [1–5,10–12,18–22,25,26]. Spontaneous breaking of TRS due to magnetism also results in the superconducting diode effect [15,16,23]. Furthermore, we can utilize the supercurrent that breaks both IS and TRS without dissipation [6,7].

In the recent study [27], an intrinsic mechanism of spontaneous IS and TRS breaking is predicted for one of the multiple superconducting phases in UTe₂ [28–34]. The competing instability of spin-triplet and spin-singlet superconductivity causes spontaneous parity mixing of Cooper pairs. In the centrosymmetric crystals such as UTe₂, the phase difference between the even-parity and odd-parity pair potentials is likely to be $\pm\pi/2$ [35], leading to the IS and TRS breaking with intact PT symmetry in the mixed-parity superconducting state. The PT-symmetric superconducting state is a novel quantum condensed phase of matter, and the realization in UTe₂ and other exotic superconductors is attracting attention. Therefore, it is eagerly desired to clarify the unique properties of the PT-symmetric superconducting states and to explore possible probes of them.

Let us classify the PT-symmetric superconducting states. In analogy with the PT-symmetric magnetic order [36], they are classified into monopole, anapole, quadrupole, and higher-order multipole superconducting states. An intriguing class is the *anapole superconductivity*, where Cooper pairs can get finite total momentum at zero magnetic field [37,38]. The anapole superconducting state is distinguished by the Fulde-Ferrell-Larkin-Ovchinnikov (FFLO) state [39,40] and the helical superconducting state [41,42], which require finite magnetic field or spin polarization. In the anapole superconductors, the finite-q pairing state is characterized by a polar vector named the effective anapole moment, which was recently revealed to arise from various origins [37,38]. On the other hand, the other classes of PT-symmetric superconducting states are nonpolar, and Cooper pairs condensate with zero total momentum. An example of them appears in the classification table for UTe₂ (see Table III), named (*magnetic*) *monopole superconductivity*. The analysis of the periodic Anderson model has shown that both anapole and monopole superconducting states are candidate superconducting states of UTe₂ [27].

An important consequence of the IS and TRS breaking is the asymmetric spectrum of Bogoliubov quasiparticles, which arises from the multiband effects in anapole and monopole superconductors [37,38]. In principle, we can distinguish all the PT-symmetric superconducting phases by the asymmetric profile of the Bogoliubov spectrum. However, the direct measurement of the Bogoliubov spectrum is challenging, especially for low-temperature superconductors. Thus, we are motivated to explore the macroscopic phenomena of anapole and monopole superconductors, especially those allowed only when symmetry breaking occurs.

For this purpose, in this paper, we study the superconducting piezoelectric effect (SCPE), a supercurrent-induced lattice distortion that occurs only when the superconductors lack both IS and TRS. We have investigated the SCPE in two-dimensional helical superconductors [43], where TRS

_____
[*]chazono.michiya.84s@st.kyoto-u.ac.jp

TABLE I. List of the irreducible representations (IRs) of the C_{2v} point group ($A_g + iB_{3u}$ anapole superconducting state) and corresponding strain s_{ij}, supercurrent J_k, and SCPE mode $d_{ijk}^{(SC)}$.

IR	Strain	Supercurrent	SCPE mode
A_1	s_{xx}, s_{yy}, s_{zz}	J_x	$d_{xxx}^{(SC)}\ d_{yyx}^{(SC)}\ d_{zzx}^{(SC)}$
A_2	s_{yz}		
B_1	s_{zx}	J_z	$d_{zxz}^{(SC)}$
B_2	s_{xy}	J_y	$d_{xyy}^{(SC)}$

TABLE III. Point group of the mixed-parity superconducting states in D_{2h} systems. For the C_{2v} point group, x, y, and z denote the principal axis.

	A_g	B_{1g}	B_{2g}	B_{3g}
A_u	D_2	$C_{2v}(z)$	$C_{2v}(y)$	$C_{2v}(x)$
B_{1u}	$C_{2v}(z)$	D_2	$C_{2v}(x)$	$C_{2v}(y)$
B_{2u}	$C_{2v}(y)$	$C_{2v}(x)$	D_2	$C_{2v}(z)$
B_{3u}	$C_{2v}(x)$	$C_{2v}(y)$	$C_{2v}(z)$	D_2

is broken by an external magnetic field. This paper focuses on the SCPE in the anapole and monopole superconductors, where IS and TRS are broken by spontaneous parity mixing in Cooper pairs without noncentrosymmetric crystal structure or external field. We also investigate the superconducting diode effect (SDE) and predict the intrinsic SDE in the anapole superconducting state, although it is absent in the monopole superconducting state. As a link of the SCPE and SDE with Cooper pairs' momentum was shown in the helical superconductors [18–20,25,43], we also discuss the properties of finite-q pairing in the anapole superconducting state for comparison. It is shown that the SCPE shows distinct behaviors depending on the origin of finite-q pairing, namely, the asymmetric Bogoliubov spectrum and quantum geometry [37,38].

This paper is organized as follows. In Sec. II, we show a minimal model for the anapole and monopole superconducting states introduced in the previous study [37] and formulate the SCPE based on the model. We also introduce the classification of possible PT-symmetric superconducting states in UTe$_2$. In Sec. III, we show numerical results of the SCPE coefficients and Cooper pairs' momentum. It is revealed that the SCPE occurs in both anapole and monopole superconducting states. The behaviors of the SCPE are closely related to the origin of the effective anapole moment, which causes finite-q pairing. We demonstrate the SDE in Sec. IV as another anomalous phenomenon in the anapole superconductors. In Sec. V, we summarize our study and discuss the future outlook.

II. FORMULATION

A. Minimal model for anapole and monopole superconducting states

We adopt a minimal model for the anapole and monopole superconducting states, which was introduced in the previous study for UTe$_2$ [37]. While UTe$_2$ has a centrosymmetric

TABLE II. List of the IRs of the D_2 point group ($A_g + iA_u$ monopole superconducting state) and corresponding strain s_{ij}, supercurrent J_k, and SCPE mode $d_{ijk}^{(SC)}$.

IR	Strain	Supercurrent	SCPE mode
A_1	s_{xx}, s_{yy}, s_{zz}		
B_1	s_{xy}	J_z	$d_{xyz}^{(SC)}$
B_2	s_{zx}	J_y	$d_{zxy}^{(SC)}$
B_3	s_{yz}	J_x	$d_{yzx}^{(SC)}$

crystal structure with D_{2h} point group symmetry, the IS is locally broken on U sites owing to the sublattice degree of freedom. Using the Nambu spinor $\hat{c}_k^T = (c_{k1\uparrow}, c_{k2\uparrow}, c_{k1\downarrow}, c_{k2\downarrow})$ where 1, 2 ($\uparrow$, $\downarrow$) denote the sublattice (spin) degree of freedom, we write the Bogoliubov-de Gennes (BdG) Hamiltonian in the following form:

$$\mathcal{H}_q = \frac{1}{2} \sum_k \begin{pmatrix} \hat{c}_{k+q}^{\dagger} & \hat{c}_{-k+q}^T \end{pmatrix} H_{BdG}(k, q) \begin{pmatrix} \hat{c}_{k+q} \\ \hat{c}_{-k+q}^* \end{pmatrix}, \quad (1)$$

$$H_{BdG}(k, q) = \begin{pmatrix} H_0(k+q) & \Delta(k)(i\sigma_y \otimes \tau_0) \\ (\Delta(k)(i\sigma_y \otimes \tau_0))^{\dagger} & -H_0(-k+q)^T \end{pmatrix}, \quad (2)$$

where τ (σ) represents the Pauli matrix vector for the sublattice (spin) degree of freedom. We here assume Cooper pairs' total momentum $2q$. The total momentum in the thermodynamically stable state is determined to minimize the free energy

$$F(q) = -\frac{T}{2} \sum_{k\alpha} \ln(1 + e^{-E_\alpha(k,q)/T}), \quad (3)$$

where E_α are eigenvalues of the BdG Hamiltonian,

$$E_\alpha(k, q) = [U^{\dagger}(k, q) H_{BdG}(k, q) U(k, q)]_{\alpha\alpha}. \quad (4)$$

Later, we show that q is finite in the anapole superconducting state while $q = 0$ in the monopole superconducting state. The normal state Hamiltonian $H_0(k)$ and superconducting order parameter $\Delta(k)$ are defined as follows.

The sublattice degree of freedom with a locally noncentrosymmetric crystal structure allows the staggered antisymmetric spin-orbit coupling (ASOC) in the centrosymmetric materials [44]. Therefore, the normal state Hamiltonian is given by

$$H_0(k) = (\varepsilon_k - \mu)\sigma_0 \otimes \tau_0 + g_k \cdot \sigma \otimes \tau_z, \quad (5)$$

where $\varepsilon_k = -2t(\cos k_x + \cos k_y + \cos k_z)$ is a kinetic energy and $g_k = (\alpha_x \sin k_y, \alpha_y \sin k_x, 0)$ represents the ASOC. Note that the relation $\alpha_y = -\alpha_x$ is not required because the local symmetry on U sites is orthorhombic C_{2v}, although it must be satisfied in the tetragonal C_{4v} systems.

We consider mixed-parity order parameters for the anapole and monopole superconducting states, and even- and odd-parity gap functions have $\pi/2$ phase difference consistent with the thermodynamic stability [35]. Because of the locally noncentrosymmetric crystal structure [44], in addition to the conventional even-parity spin-singlet and odd-parity spin-triplet pairings, even-parity spin-triplet and odd-parity
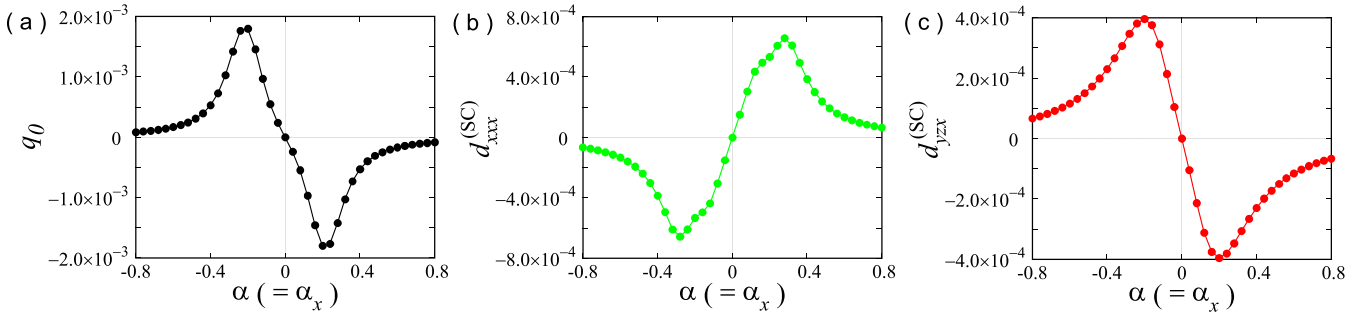
FIG. 1. Results of the group velocity model: $\alpha(=\alpha_x)$ dependence of (a) q_0, (b) $d_{xxx}^{(SC)}$ in the $A_g + iB_{3u}$ anapole state, and (c) $d_{yzx}^{(SC)}$ in the $A_g + iA_u$ monopole state. We set $\alpha_y = 0$, $\beta = 1$, and $T = 0.01$.

spin-singlet pairings can be finite. To satisfy the fermion's anticommutation relation, the superconducting order parameter is given by

$$\Delta(\boldsymbol{k}) = \Delta_1\left(\psi_{\boldsymbol{k}}^g \sigma_0 \otimes \tau_0 + \beta \boldsymbol{d}_{\boldsymbol{k}}^g \cdot \boldsymbol{\sigma} \otimes \tau_z\right)$$
$$+ \Delta_2\left(\psi_{\boldsymbol{k}}^u \sigma_0 \otimes \tau_z + \boldsymbol{d}_{\boldsymbol{k}}^u \cdot \boldsymbol{\sigma} \otimes \tau_0\right), \quad (6)$$

where $\psi_{\boldsymbol{k}}^{g(u)}$ is an even-parity (odd-parity) spin-singlet component and $\boldsymbol{d}_{\boldsymbol{k}}^{g(u)}$ is an even-parity (odd-parity) spin-triplet component of the gap function. In this paper, we assume the even-parity component belonging to the A_g irreducible representation, specifically, $\psi_{\boldsymbol{k}}^g = 1$ and $\boldsymbol{d}_{\boldsymbol{k}}^g = (0, \sin k_x, 0)$. For the odd-parity component, B_{3u} and A_u irreducible representations are examined. For simplicity, $\psi_{\boldsymbol{k}}^u = 0$ is ignored, and we consider spin-triplet pairing with $\boldsymbol{d}_{\boldsymbol{k}}^u = (0, 0, \sin k_y)$ and $\boldsymbol{d}_{\boldsymbol{k}}^u = (0, 0, \sin k_z)$, corresponding to the B_{3u} and A_u representations, respectively. We choose a real Δ_1 and a pure imaginary Δ_2 without loss of generality. The coexistent $A_g + iB_{3u}$ state and $A_g + iA_u$ state realize the anapole and monopole superconductivity, as discussed in the next subsection. These states are predicted in a microscopic analysis of the periodic Anderson model for UTe$_2$ [27]. However, the following results are expected to be general in the sense that the main conclusion for the SCPE and SDE applies to other representations, such as the $A_g + iB_{1u}$ state, and other candidate materials as well. For a later discussion, in Eq. (6) we introduce β as the strength of the staggered spin-triplet gap function allowed in locally noncentrosymmetric superconductors [44]. We will see that β is an important parameter for the superconducting properties.

B. Superconducting piezoelectric effect (SCPE)

The SCPE is defined as a lattice distortion induced by a supercurrent [43]. In the linear response regime, it is formulated as follows:

$$s_{ij} = d_{ijk}^{(SC)} J_k, \quad (7)$$

where s_{ij} is a strain tensor, $d_{ijk}^{(SC)}$ is a SCPE coefficient, and J_k is a supercurrent. Because s_{ij} (J_k) is a parity even (odd) and time-reversal even (odd) quantity, $d_{ijk}^{(SC)}$ can be finite only in systems lacking both IS and TRS.

The structure of the SCPE tensor $d_{ijk}^{(SC)}$ depends on the point group of the superconducting states. For a coefficient $d_{ijk}^{(SC)}$ to be finite, corresponding s_{ij} and J_k must belong to the same irreducible representation. Let us consider the cases of our model. The point group of the $A_g + iB_{3u}$ state is polar C_{2v}, while that of the $A_g + iA_u$ state is nonpolar D_2. Thus, the former is the anapole superconducting state and the latter is the monopole superconducting state in analogy with the classification of magnetic states [45]. The classification of the strain s_{ij} and supercurrent J_k based on the C_{2v} and D_2 point group is summarized in Tables I and II, respectively. The SCPE modes allowed by symmetry are also shown in the tables. We show the classification of PT-symmetric superconducting states in Table III and see that all the PT-symmetric superconducting states belong to either C_{2v} or D_2 point group in the orthorhombic D_{2h} system. Thus, the classification in Tables I and II applies the other states as well, when we choose an appropriate twofold rotation axis for C_{2v} (See Appendix A for the complete results).
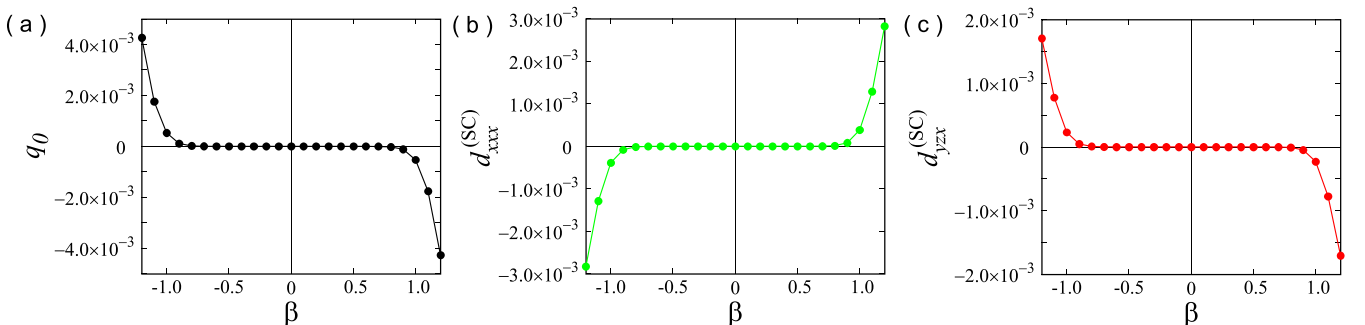

FIG. 2. Results of the group velocity model: β dependence of (a) q_0, (b) $d_{xxx}^{(SC)}$ in the $A_g + iB_{3u}$ anapole state, and (c) $d_{yzx}^{(SC)}$ in the $A_g + iA_u$ monopole state. We set $\alpha_y = 0$, $\alpha(=\alpha_x) = 0.4$, and $T = 0.01$.
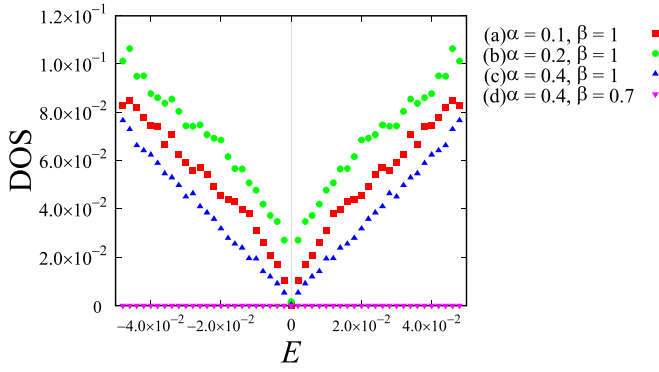
FIG. 3. The DOS in the group velocity model for the $A_g + iB_{3u}$ anapole state. The parameters are (a) $\alpha(=\alpha_x) = 0.1$, $\beta = 1$, (b) $\alpha = 0.2$, $\beta = 1$, (c) $\alpha = 0.4$, $\beta = 1$, and (d) $\alpha = 0.4$, $\beta = 0.7$. We assume $\alpha_y = 0$ and set $q_0 = 0$ for simplicity.

For the estimation of the strain, we calculate the expectation values of the weighted density operator, which characterizes the modulation of the hopping parameters due to the distortion [36,43]. Although the strain is proportional to the weighted density, we avoid calculating the proportionality coefficient because it strongly depends on material parameters, such as electron-phonon coupling and elastic modulus. The weighted density operator is defined as

$$\hat{n}_{ij} = \sum_{\boldsymbol{k}} \begin{pmatrix} \hat{c}^{\dagger}_{\boldsymbol{k}+\boldsymbol{q}} & \hat{c}^{T}_{-\boldsymbol{k}+\boldsymbol{q}} \end{pmatrix} n_{ij}(\boldsymbol{k},\boldsymbol{q}) \begin{pmatrix} \hat{c}_{\boldsymbol{k}+\boldsymbol{q}} \\ \hat{c}^{*}_{-\boldsymbol{k}+\boldsymbol{q}} \end{pmatrix}, \quad (8)$$

$$n_{ij}(\boldsymbol{k},\boldsymbol{q}) = \frac{1}{2} \begin{pmatrix} D_{ij}(\boldsymbol{k}+\boldsymbol{q}) \times I_4 & 0 \\ 0 & -D_{ij}(-\boldsymbol{k}+\boldsymbol{q}) \times I_4 \end{pmatrix}, \quad (9)$$

$$D_{ij}(\boldsymbol{k}) = \begin{cases} \cos k_i & (i = j) \\ \sin k_i \sin k_j & (i \neq j) \end{cases}, \quad (10)$$

and expectation values are calculated by

$$\langle \hat{n}_{ij} \rangle_{\mathrm{eq},\boldsymbol{q}}$$
$$= \frac{1}{V} \sum_{\boldsymbol{k}\alpha} [U^{\dagger}(\boldsymbol{k},\boldsymbol{q}) n_{ij}(\boldsymbol{k},\boldsymbol{q}) U(\boldsymbol{k},\boldsymbol{q})]_{\alpha\alpha} f(E_{\alpha}(\boldsymbol{k},\boldsymbol{q})), \quad (11)$$

where $f(E) = (e^{E/T} + 1)^{-1}$ is the Fermi distribution function. We calculate the expectation value of the supercurrent

in a similar way,

$$\langle \hat{J}_k \rangle_{\mathrm{eq},\boldsymbol{q}}$$
$$= \frac{1}{V} \sum_{\boldsymbol{k}\alpha} [U^{\dagger}(\boldsymbol{k},\boldsymbol{q}) J_k(\boldsymbol{k},\boldsymbol{q}) U(\boldsymbol{k},\boldsymbol{q})]_{\alpha\alpha} f(E_{\alpha}(\boldsymbol{k},\boldsymbol{q})), \quad (12)$$

where

$$J_k(\boldsymbol{k},\boldsymbol{q}) = \frac{e}{2} \begin{pmatrix} \partial_{k_k} H_0(\boldsymbol{k}+\boldsymbol{q}) & 0 \\ 0 & -\partial_{k_k} H_0(-\boldsymbol{k}+\boldsymbol{q}) \end{pmatrix}. \quad (13)$$

Then, we redefine the SCPE coefficient $d_{ijk}^{(\mathrm{SC})}$ by

$$d_{ijk}^{(\mathrm{SC})} = \lim_{q_k' \to 0} \frac{\langle \hat{n}_{ij} \rangle_{\mathrm{eq},\boldsymbol{q}+q_k'} - \langle \hat{n}_{ij} \rangle_{\mathrm{eq},\boldsymbol{q}-q_k'}}{\langle \hat{J}_k \rangle_{\mathrm{eq},\boldsymbol{q}+q_k'} - \langle \hat{J}_k \rangle_{\mathrm{eq},\boldsymbol{q}-q_k'}}, \quad (14)$$

where q_k' is Cooper pairs' momentum parallel to the supercurrent J_k.

C. Classification of anapole superconducting states

In the previous section, the superconducting states have been classified based on symmetry. Here, we furthermore classify the anapole superconducting states by their microscopic properties.

The effective anapole moment in the superconducting state is defined by the first derivative of thermodynamic potential with respect to the Cooper pairs' momentum [37], and thus, finite anapole moment directly indicates the finite-q pairing state. As clarified in our recent paper, there exist several origins of the effective anapole moment [38]. They are classified into the group velocity term and the geometric term. While the former arises from the asymmetric Bogoliubov spectrum as pointed out in the previous study [37], the latter is induced by the quantum geometric effect, which has recently attracted attention in various fields [46–61]. Owing to the geometric term, the finite-q pairing state can be stabilized even for an ordinary quasiparticle's spectrum, where neither the asymmetry nor the Zeeman splitting exists. Thus, the anapole superconducting states can be classified into three cases: The anapole moment is owing to (A) purely group velocity term, (B) purely geometric term, and (C) cooperation of the two terms.

The three cases can be represented in our model by choosing the following parameters:

(A) $\alpha_y = 0$ and $\beta \neq 0$ (group velocity model),

(B) $\alpha_y \neq 0$ and $\beta = 0$ (geometric effect model),
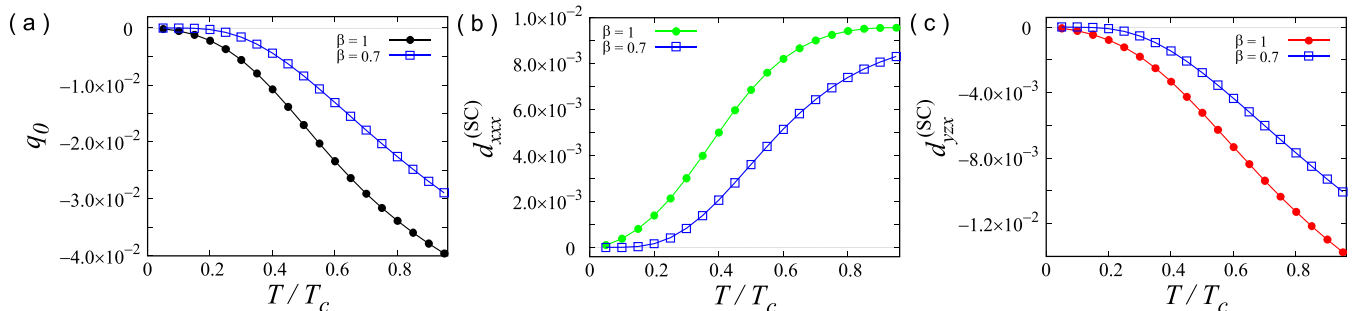
(C) $\alpha_y \neq 0$ and $\beta \neq 0$ (mixed model).

FIG. 4. Results of the group velocity model: Temperature dependence of (a) q_0, (b) $d_{xxx}^{(\mathrm{SC})}$ in the $A_g + iB_{3u}$ anapole state, and (c) $d_{yzx}^{(\mathrm{SC})}$ in the $A_g + iA_u$ monopole state. We set $\alpha_y = 0$, $\alpha(=\alpha_x) = 0.4$, and $\beta = 1$ or 0.7.
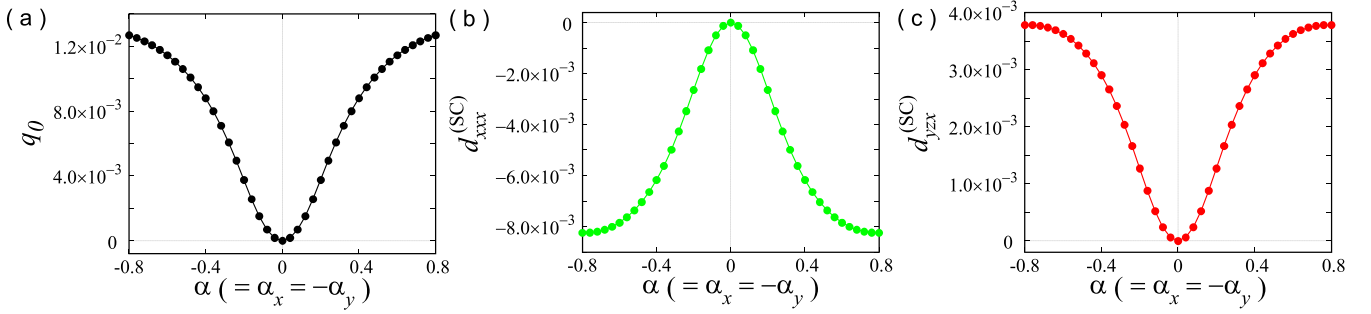
FIG. 5. Results of the geometric effect model: α dependence of (a) q_0, (b) $d_{xxx}^{(SC)}$ in the $A_g + iB_{3u}$ anapole state, and (c) $d_{yzx}^{(SC)}$ in the $A_g + iA_u$ monopole state. We set $\alpha = \alpha_x = -\alpha_y$, $\beta = 0$, and $T = 0.01$.

In the group velocity model, the group velocity term is finite while the geometric term vanishes. In contrast, the group velocity term vanishes in the geometric effect model. Both the group velocity and geometric terms are finite in the mixed model. In the next section, we show that the behaviors of the SCPE are different between the three cases.

In this study, we adopt the following parameters unless we explicitly state otherwise: $t = 1$, $\mu = -4$, $\Delta_1(T) = 0.2\sqrt{1 - (T/T_c)}$, $\Delta_2(T) = 0.2i\sqrt{1 - (T/T_c)}$ (namely, $|\Delta_2| = \Delta_1$), and the transition temperature is $T_c = 0.1$.

III. RESULT : SCPE

In this section, we show the numerical results of the Cooper pairs' momentum $\boldsymbol{q} = (q_0, 0, 0)$, the SCPE coefficient $d_{xxx}^{(SC)}$ in the $A_g + iB_{3u}$ anapole state, and $d_{yzx}^{(SC)}$ in the $A_g + iA_u$ monopole state. Because we find $\boldsymbol{q} = 0$ in the monopole state, we show q_0 only for the anapole state. We discuss the $\alpha(= \alpha_x)$, β, and T dependence of the SCPE in the three models introduced in the previous section (Sec. II C) and compare them with the Cooper pairs' momentum in the anapole superconducting state. A close relation between the SCPE and Cooper pairs' momentum is revealed.

A. Group velocity model

First, we analyze the group velocity model, where we set $\alpha_y = 0$ and $\beta \neq 0$. In this model, the effect of the quantum geometry of Bloch states is negligible. The α and β dependencies of $d_{ijk}^{(SC)}$ are shown in Figs. 1 and 2, together with the Cooper pairs' momentum q_0 in the anapole state. It is shown that the SCPE coefficients are finite in the anapole and monopole superconducting states and their magnitudes are comparable. Thus, we see the SCPE in the PT-symmetric superconducting states, irrespective of whether the Cooper pairs' momentum is finite or zero.

On the other hand, we notice similarities between the SCPE and Cooper pairs' momentum by comparing the parameter dependence of $d_{ijk}^{(SC)}$ and q_0. In particular, these quantities are antisymmetric with respect to α and β. The antisymmetric behavior of q_0 is expected from the result of the anapole moment T_x [38] because the relation $q_0 \approx -T_x/D_{xx}$ holds with D_{xx} being the superfluid weight and T_x is α (β) antisymmetric in this model. On the other hand, it is nontrivial that $d_{ijk}^{(SC)}$ is also antisymmetric. We can interpret the similarities by analogy with the magnetopiezoelectric effect [36,62,63], the

counterpart of the SCPE in the normal state. It was shown that the magnetopiezoelectric effect originates from the asymmetric Fermi surface [36]. In the group velocity model, the Cooper pairs' momentum arises from the asymmetric spectrum. Therefore, it is reasonable that the SCPE and Cooper pairs' momentum show similar behaviors. Indeed, their antisymmetric behaviors with respect to α and β are explained as follows. The Bogoliubov spectrum is asymmetric and it is reversed by changing the sign of α or β in this model (see Appendix B). Since the SCPE and Cooper pairs' momentum are caused by the asymmetric spectrum, it is natural that reversing spectrum changes the sign of $d_{ijk}^{(SC)}$ and q_0. We stress that this interpretation is valid even for the monopole state.

Furthermore, $d_{ijk}^{(SC)}$ and q_0 show a similar peak structure around $\alpha = \pm 0.2$ and drastically change around $\beta = \pm 1$. These behaviors are related to the density of states (DOS) in the low-energy region, which is shown for the $A_g + iB_{3u}$ anapole state with several parameters (Fig. 3). Note that the DOS in Fig. 3 is calculated with $q_0 = 0$ for simplicity. Parameters leading to larger DOS around the Fermi level $E = 0$ correspond to larger q_0 and $d_{ijk}^{(SC)}$. This is consistent with the fact that the asymmetric spectrum is the main source of both q_0 and $d_{ijk}^{(SC)}$. It is also indicated that thermally excited quasiparticles are essential. In Fig. 3, we see that the low-energy Bogoliubov spectrum is sensitive to the parameter β. With our parameter set, the spectrum is fully gapped for $|\beta| < 1$ while the nodal spectrum appears with $|\beta| \geqslant 1$. To be more precise, point nodes are present at $\beta = 1$, and when $\beta > 1$, the Bogoliubov Fermi surface appears (see Appendix B), which has been studied with interest in the topological nature [64–66]. Thus, the low-energy DOS increases for $\beta \geqslant 1$, and therefore, the SCPE and Cooper pairs' momentum are enhanced.

Based on the above discussion, we expect a notable temperature dependence reflecting the gap structure. Indeed, a characteristic behavior is observed in the temperature dependence of q_0 and $d_{ijk}^{(SC)}$, which are suppressed in the low-temperature region (Fig. 4). In Ref. [38], it is shown that the asymmetry of the Bogoliubov spectrum is reflected in the anapole moment through the Fermi distribution function as $f(E(\boldsymbol{k})) - f(E(-\boldsymbol{k}))$, and therefore, the anapole moment and q_0 are suppressed in the low-temperature region of gapped states. The SCPE is expected to be suppressed by the same mechanism. Indeed, the SCPE shows exponential temperature dependence in the full-gapped state ($\beta = 0.7$) while
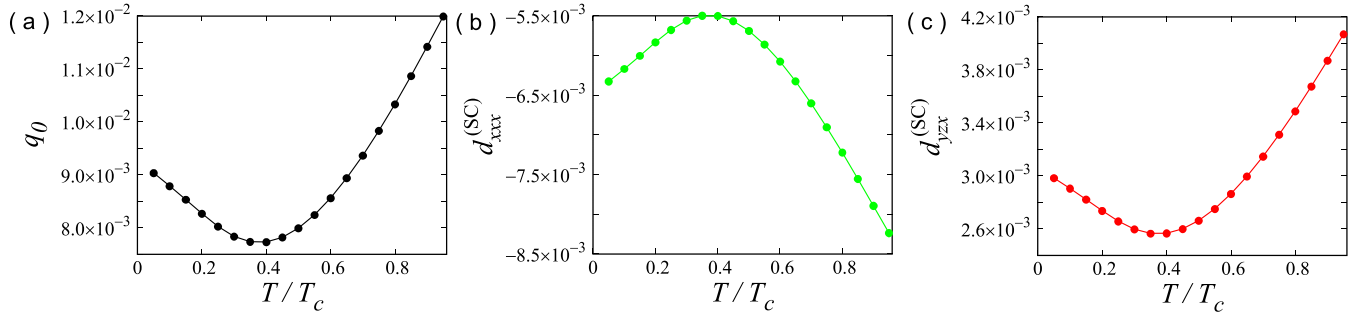
FIG. 6. Results of the geometric effect model: Temperature dependence of (a) q_0, (b) $d_{xxx}^{(SC)}$ in the $A_g + iB_{3u}$ anapole state, and (c) $d_{yzx}^{(SC)}$ in the $A_g + iA_u$ monopole state. We set $\alpha (= \alpha_x = -\alpha_y) = 0.4$ and $\beta = 0$.

it shows power-law dependence in the nodal state ($\beta = 1$). These results support the fact that the SCPE in the group velocity model relies on the asymmetric energy spectrum, like the magnetopiezoelectric effect in the odd-parity magnetic ordered states [36,62,63]. Hereafter, we call this mechanism of SCPE "asymmetric origin" named after the asymmetric Bogoliubov spectrum.

Note that we assume the second-order superconducting transition and thus the order parameters $\Delta_{1(2)}(T)$ smoothly become zero at $T = T_c$ (see Sec. II C). As shown in Fig. 4, $d_{ijk}^{(SC)}$ and q_0 are sizable at just below T_c. Later we will see the same property in the geometric effect model and mixed model. Large q_0 near the transition temperature was also reported for the helical superconducting state [19,25].

B. Geometric effect model

Second, we set $\alpha_y = -\alpha_x (= -\alpha)$ and $\beta = 0$, in which the origin of the effective anapole moment is the geometric term since the group velocity term disappears. Note that the point group of the monopole superconducting state with this parameter set is D_4, leading to the constraints $d_{xyz}^{(SC)} = 0$ and $d_{yzx}^{(SC)} = -d_{zxy}^{(SC)}$.

The α dependence of q_0 and $d_{ijk}^{(SC)}$ is shown in Fig. 5, which reveals the finite SCPE in the geometric effect model. However, in contrast to the group velocity model, the Bogoliubov spectrum is symmetric in this model for $q_0 = 0$ (see Appendix C). Indeed, $q_0 = 0$ in the monopole state and the spectrum is symmetric as $E_\alpha(\boldsymbol{k}) = E_\alpha(-\boldsymbol{k})$. Therefore, the origin of the SCPE must be different from the group

velocity model where the asymmetric spectrum causes the SCPE. The geometric effect model also shows a similar parameter dependence of the Cooper pairs' momentum and the SCPE coefficients. Considering the fact that the anapole moment arises from the quantum geometry in this model [38], the similarity implies that the quantum geometry plays an essential role also in the SCPE. The α-symmetric behavior of the SCPE coefficients $d_{ijk}^{(SC)}$ is consistent with this interpretation because the quantum geometry induces the α symmetric anapole moment in the geometric effect model [38].

The above discussion is supported by the temperature dependence of q_0 and $d_{ijk}^{(SC)}$ plotted in Fig. 6. Although there is a sizable energy gap in the spectrum (see Appendix C), the SCPE and Cooper pairs' momentum are sizable even at low temperatures, in contrast to the group velocity model (Fig. 4). Indeed, the temperature dependence of q_0 and $d_{ijk}^{(SC)}$ are weak. This behavior is consistent with the above discussion because the effect of the quantum geometry of Bloch electrons is not suppressed by the energy gap. Hereafter, we call this case of the SCPE "symmetric origin" named after the symmetric Bogoliubov spectrum.

Here, we make a brief comment on the temperature dependence in the geometric effect model. We can see broad minimum and maximum of q_0 and $d_{ijk}^{(SC)}$ in Fig. 6. Since similar temperature dependence appears for other several parameter sets, these behaviors may be characteristic of the quantum geometric effect. However, we do not touch on such a weak temperature dependence in the following discussions since it is not related to the main conclusion.
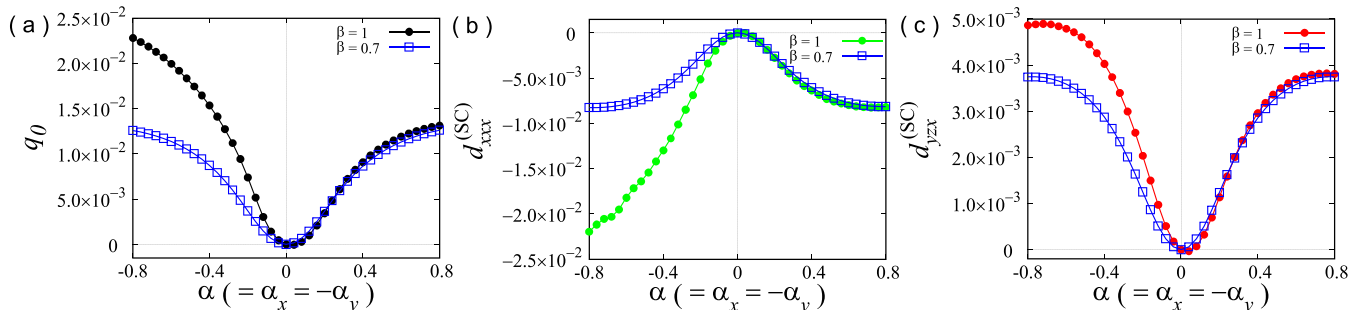

FIG. 7. Results of the mixed model: α dependence of (a) q_0, (b) $d_{xxx}^{(SC)}$ in the $A_g + iB_{3u}$ anapole state, and (c) $d_{yzx}^{(SC)}$ in the $A_g + iA_u$ monopole state. We set $\alpha = \alpha_x = -\alpha_y$, $\beta = 1$ or 0.7, and $T = 0.01$.
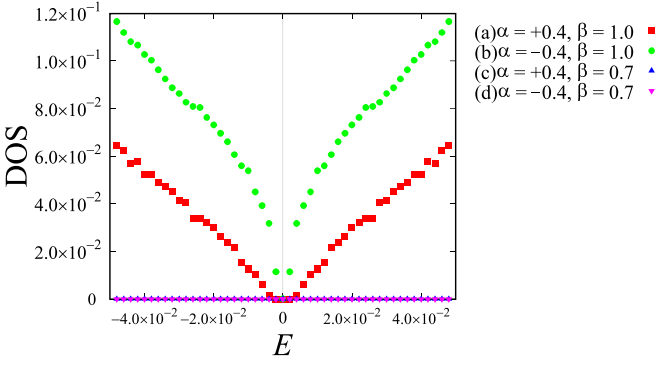
FIG. 8. The DOS in the $A_g + iB_{3u}$ anapole state with the following parameters: (a) $\alpha(=\alpha_x=-\alpha_y) = +0.4$, $\beta = 1$, (b) $\alpha = -0.4$, $\beta = 1$, (c) $\alpha = +0.4$, $\beta = 0.7$, and (d) $\alpha = -0.4$, $\beta = 0.7$. We set $q_0 = 0$ for simplicity.

C. Mixed model

Finally, we set $\alpha_y = -\alpha_x(=-\alpha)$ and $\beta \neq 0$, where both the group velocity term and the geometric term contribute to the effective anapole moment. As shown in Fig. 7, the α dependence of q_0 and $d_{ijk}^{(SC)}$ is asymmetric for $\beta = 1$, although it is almost symmetric for $\beta = 0.7$. We can interpret these features based on the results in the previous subsections: Since q_0 and $d_{ijk}^{(SC)}$ are very small in the group velocity model for $|\beta| < 1$ (Fig. 2), the SCPE of the asymmetric origin is naturally small in the mixed model. Thus, the SCPE mainly arises from the symmetric origin, consistent with the α-symmetric behavior similar to the geometric effect model (Fig. 5). On the other hand, the asymmetric origin gives rise to a sizable contribution to the SCPE when $|\beta| \geqslant 1$, making the SCPE asymmetric with respect to α.

As we discussed for the group velocity model, the SCPE of the asymmetric origin is related to the DOS. This is correct in the mixed model as well. Figure 8 shows the DOS in the mixed model. First, we see that the superconducting gap suppresses the low-energy DOS for $\beta = 0.7$, consistent with the negligible contribution to the SCPE by the asymmetric origin. Second, we see sizable DOS for $\beta = 1$, and it is larger for $\alpha = -0.4$ than for $\alpha = 0.4$. Thus, it is indicated that the SCPE of the asymmetric origin is suppressed for $\alpha > 0$ because of the small low-energy DOS. In other words, we see a

significant contribution of the asymmetric origin when $\beta \geqslant 1$ and $\alpha < 0$. This is consistent with the parameter dependence of the SCPE in Fig. 7.

The β dependence also supports the above discussion. Note that the parameter sets $(\alpha_x, \alpha_y, \beta)$ and $(-\alpha_x, -\alpha_y, -\beta)$ give the same results in our model. Figure 9 shows the β dependence of the SCPE coefficients for $\alpha = 0.4$. The drastic change around $\beta = -1$ is attributed to the sizable DOS, which is equivalent to that for $(\alpha, \beta) = (-0.4, 1)$. Figure 9 also reveals that the SCPE of the symmetric origin is nearly β independent.

The SCPE in the mixed model may show a unique temperature dependence as a consequence of the competition between the asymmetric and symmetric origins. As shown in Figs. 10(a) and 10(c), q_0 and $d_{yzx}^{(SC)}$ change the sign at a certain temperature. The sign reversal occurs because the temperature dependence is significantly different between the SCPE of the asymmetric origin and that of the symmetric origin (compare Fig. 4 with Fig. 6). When the superconducting state is gapped, the SCPE is dominated by the symmetric origin at low temperatures, and thus, the quantum geometry is expected to play an essential role. On the other hand, the asymmetric origin related to the asymmetric Bogoliubov spectrum gives a large contribution near the transition temperature, and it can cause the sign change. Note that the sign reversal is not a general property, and it is sensitive to the detail of the system and SCPE mode. Indeed, there is no sign change in $d_{xxx}^{(SC)}$ [see Fig. 10(b)], for instance.

It should be noticed that the Cooper pairs' momentum q_0 and the SCPE coefficients $d_{ijk}^{(SC)}$ show similar behaviors in all the models and parameters studied in this paper. This is also the case of the helical superconducting state studied earlier [43]. Surprisingly, this correspondence applies to the SCPE in the monopole superconducting state as well. Although $q_0 = 0$ in the monopole state, the SCPE shows a similar parameter dependence to q_0 in the anapole state. From these results, we suppose that the SCPE arises from the asymmetric Bogoliubov spectrum and quantum geometry like the anapole moment [38]. Further analysis of the SCPE related to quantum geometry is left as a future issue.

IV. FIELD-FREE DIODE EFFECT

In this section, we demonstrate the field-free SDE in the anapole superconductors, which means the nonreciprocity in
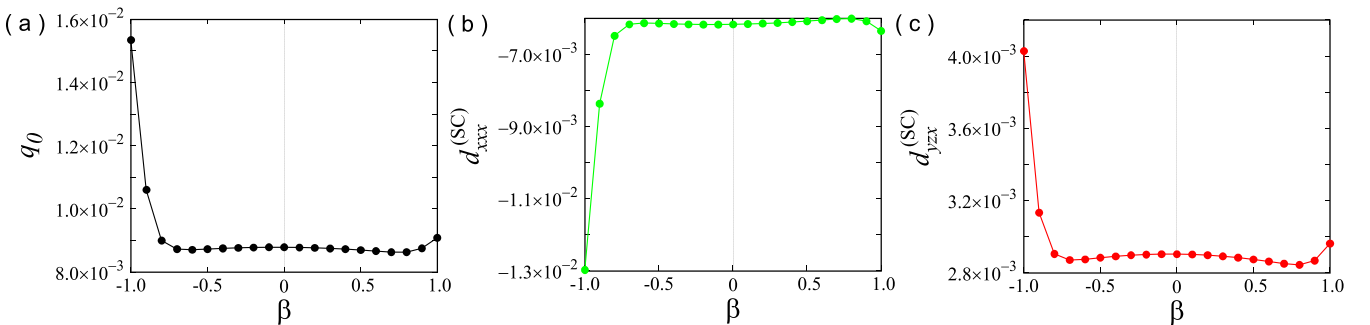

FIG. 9. Results of the mixed model: β dependence of (a) q_0, (b) $d_{xxx}^{(SC)}$ in the $A_g + iB_{3u}$ anapole state, and (c) $d_{yzx}^{(SC)}$ in the $A_g + iA_u$ monopole state. We set $\alpha(=\alpha_x=-\alpha_y) = 0.4$ and $T = 0.01$.
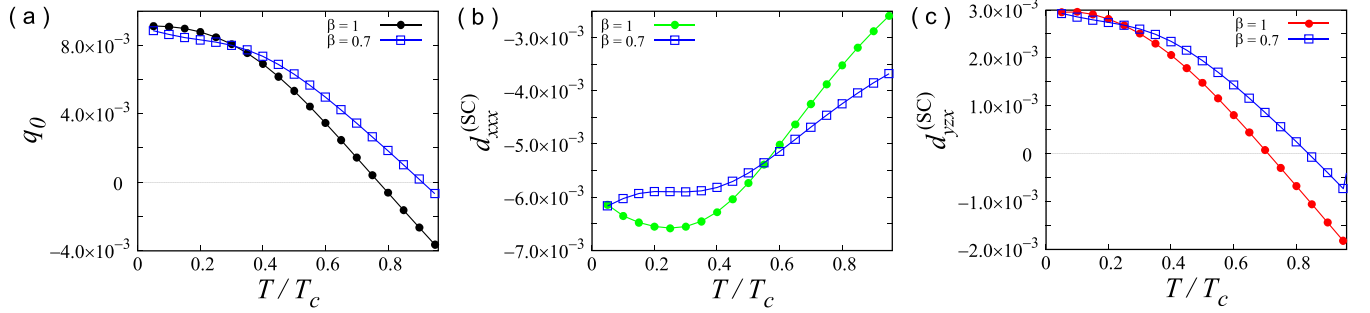
FIG. 10. Results of the mixed model: Temperature dependence of (a) q_0, (b) $d_{xxx}^{(SC)}$ in the $A_g + iB_{3u}$ anapole state, and (c) $d_{yzx}^{(SC)}$ in the $A_g + iA_u$ monopole state. We set $\alpha (= \alpha_x = -\alpha_y) = 0.4$ and $\beta = 1$ or 0.7.

the critical current in the absence of the magnetic field. Here, we consider the SDE along the x axis with the $A_g + iB_{3u}$ anapole superconducting state in mind. Adopting the formulation for the intrinsic SDE [19], we calculate the depairing critical current as

$$J_{c+} = \max_{q_x} \langle \hat{J}_x \rangle_{\mathrm{eq}, q_x}, \quad J_{c-} = \min_{q_x} \langle \hat{J}_x \rangle_{\mathrm{eq}, q_x}, \qquad (15)$$

using Eq. (12). The q_x dependence of $\langle \hat{J}_x \rangle_{\mathrm{eq}, q_x}$ in the $A_g + iB_{3u}$ anapole state is shown in Fig. 11 for example, by which we determine J_{c+} and J_{c-}. The nonreciprocal component of the critical current is given by

$$\Delta J_c = J_{c+} + J_{c-}, \qquad (16)$$

and the SDE efficiency is defined as

$$r = \Delta J_c / \bar{J}_c, \qquad (17)$$

with $\bar{J}_c = (J_{c+} - J_{c-})/2$.

The numerical results of ΔJ_c and r are shown in Figs. 12 and 13, respectively. We obtain finite nonreciprocity in the critical current characterized by ΔJ_c and r in all the models for the anapole superconducting states, namely, the (A) group velocity model, (B) geometric effect model, and (C) mixed model. Thus, the field-free SDE is a ubiquitous feature of anapole superconductors. It is shown that ΔJ_c is suppressed
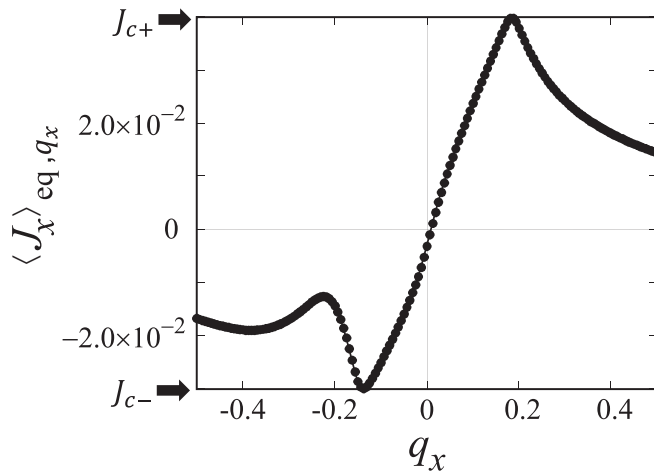

FIG. 11. Supercurrent $\langle \hat{J}_x \rangle_{\mathrm{eq}, q_x}$ as a function of q_x in the mixed model of the $A_g + iB_{3u}$ anapole state. We set $\alpha = \alpha_x = -\alpha_y = 0.4$, $\beta = 1$, and $T = 0.01$. Critical currents J_{c+} and J_{c-} are marked by arrows.

monotonically with increasing temperature. This behavior is in stark contrast to the fact that the temperature dependence of Cooper pairs' momentum q_0 and SCPE coefficients significantly depends on the model. Note that the temperature scaling around $T = T_c$ is not reliable because the q dependence of the magnitude of gap function is neglected in our calculation, while it is negligible and the results are reliable at low temperatures [19]. Interestingly, the SDE efficiency r reaches 40%, which is comparable to the maximum value in the helical superconducting state at high magnetic fields [19]. Thus, our results suggest a sizable SDE in the anapole superconducting state at the zero magnetic field. The SDE along the x axis is allowed only in the anapole state, and it vanishes in the monopole state. Generally speaking, the SDE occurs in the anapole state with supercurrent in the same direction as the Cooper pairs' momentum q_0. Therefore, the SDE is suitable as a probe to distinguish the anapole and monopole states and to determine the direction of the anapole moment.

V. SUMMARY AND DISCUSSION

In this paper, we formulated and demonstrated the superconducting piezoelectric effect (SCPE) in the anapole and monopole superconducting states. We also showed the field-free superconducting diode effect (SDE) in the anapole superconducting state. The spontaneous IS and TRS breaking in these PT-symmetric superconducting states allows the off-diagonal and nonreciprocal responses without external symmetry-breaking fields. Therefore, the SCPE and SDE directly reflect the symmetry of superconducting states, and they can be used for probing the exotic symmetry and topology of superconductors. In particular, the SCPE occurs under all the symmetry groups lacking the IS and TRS. Thus, in principle, we can distinguish the symmetry of superconducting states by the analysis of the SCPE tensor. For instance, we provided the classification table for the SCPE tensor in the D_{2h} point group, corresponding to the candidate superconductor UTe$_2$. On the other hand, the field-free SDE occurs only along the anapole moment in the anapole superconducting state. Therefore, the observation of the SDE may evidence the anapole superconductivity and determine the direction of the anapole moment.

Our calculations revealed the close relationship between the SCPE and the Cooper pairs' momentum. In the anapole state, the Cooper pairs can get finite momentum like in the FFLO and helical superconducting states, and the momentum is proportional to the anapole moment. In our results, the
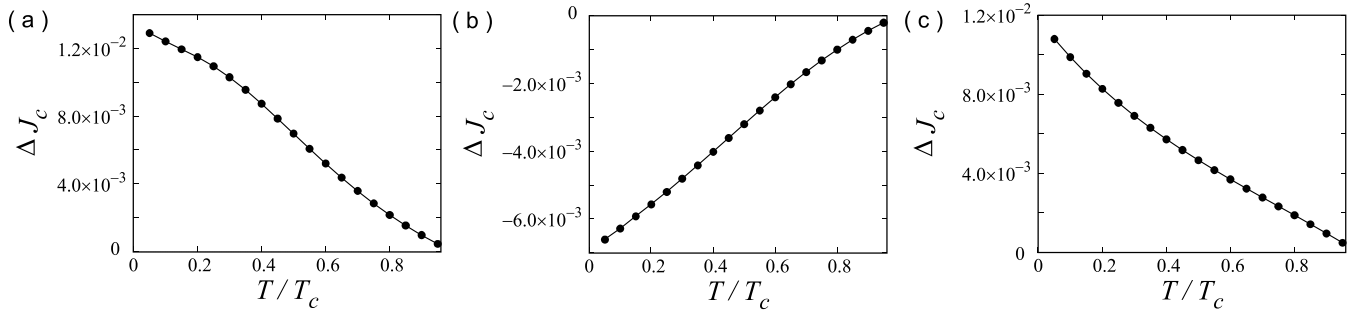
FIG. 12. Temperature dependence of the nonreciprocal critical current ΔJ_c in the (a) group velocity model, (b) geometric effect model, and (c) mixed model of the $A_g + iB_{3u}$ anapole state. The parameters (α, β) are (a) (0.4,1), (b) (0.4,0), and (c) (0.4,1) as in Figs. 4, 6, and 10.

SCPE coefficients show similar parameter dependence to the Cooper pairs' momentum. According to our recent studies [37,38], the anapole moment and Cooper pairs' momentum may have several origins, namely, the asymmetric spectrum of Bogoliubov quasiparticles and quantum geometry of Bloch electrons. The similarity implies the same origins of the SCPE. Interestingly, the relation is confirmed between the SCPE in the monopole state and Cooper pairs' momentum in the anapole state. To clarify the microscopic origin of the SCPE, further theoretical analysis is desired and remains to be a future issue.

On the other hand, the SDE looks unrelated to the Cooper pairs' momentum unlike the results of the helical superconducting state [19,25]. Therefore, the SDE is unlikely to be used for a probe of the magnitude of Cooper pairs' momentum. A characteristic property of the anapole superconducting state is that the SDE occurs at the zero magnetic field. Such field-free SDE has been searched in the recent research of SDE, but the platform is limited at present [14–16,23]. Anapole superconductors are a platform of field-free SDE without symmetry-breaking magnetic order or external fields. The rectified supercurrent is parallel to the momentum of Cooper pairs. In our calculation, a large SDE quality factor over 40% is obtained.

We expect that the SCPE and SDE will be complementary to other observable quantities characterizing the exotic superconducting states. For instance, our recent paper [38] proposed a phenomenon specific to the anapole superconductor, the temperature-dependent Bogoliubov Fermi surface. The Bogoliubov Fermi surface affects thermodynamic properties [67–69], which could be experimentally verified, in

principle. On the other hand, the SCPE and SDE occur regardless of the presence or absence of the Bogoliubov Fermi surface.

An intriguing future task is to examine the SCPE and SDE in UTe$_2$, a candidate of the anapole and monopole superconductivity. A recent ultrasound measurement detected softening of the elastic mode corresponding to the strain s_{zx} [70]. Thus, it is expected that the corresponding SCPE mode is enhanced. That is the B_1 mode in the anapole superconducting state while the B_2 mode in the monopole superconducting state. The former is induced by the supercurrent along the z axis, and it is along the y axis in the latter.

APPENDIX A: SYMMETRY ANALYSIS OF *PT*-SYMMETRIC SUPERCONDUCTING STATES AND SCPE BASED ON THE POINT GROUP D_{2h}

We discuss the anapole and monopole superconducting states classified based on the D_{2h} point group. There are four even-parity and four odd-parity irreducible representations in the D_{2h} point group, and accordingly, their coexistence allows sixteen mixed-parity superconducting states. The classification of superconducting states is summarized in Table III.
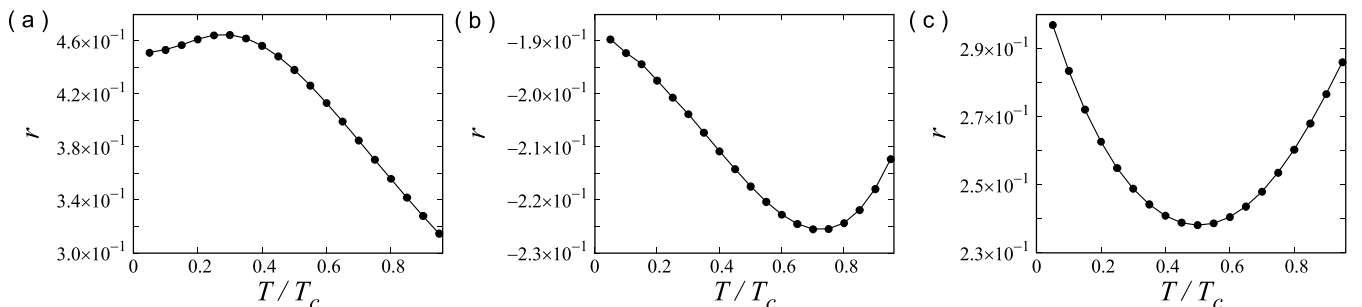

FIG. 13. Temperature dependence of the SDE efficiency r in the (a) group velocity model, (b) geometric effect model, and (c) mixed model of the $A_g + iB_{3u}$ anapole state. The parameters (α, β) are (a) (0.4,1), (b) (0.4,0), and (c) (0.4,1) as in Figs. 4, 6, and 10.

TABLE IV. List of the IRs of the $C_{2v}(y)$ anapole superconducting state and corresponding strain s_{ij}, supercurrent J_k, and SCPE mode $d_{ijk}^{(SC)}$.

IR	Strain	Supercurrent	SCPE modes		
A_1	s_{xx}, s_{yy}, s_{zz}	J_y	$d_{xxy}^{(SC)}$	$d_{yyy}^{(SC)}$	$d_{zzy}^{(SC)}$
A_2	s_{zx}				
B_1	s_{xy}	J_x	$d_{xyx}^{(SC)}$		
B_2	s_{yz}	J_z	$d_{yzz}^{(SC)}$		

In the mixed-parity superconducting states, the point group symmetry is reduced from the normal state point group (D_{2h}) owing to the spontaneous parity violation. For instance, the point group of the $B_{1g} + iB_{3u}$ state is C_{2v} with the principal axis in the y direction. This means that the $B_{1g} + iB_{3u}$ state is an anapole superconducting state, where Cooper pairs can get total momentum in the y direction, $\boldsymbol{q} = (0, q_0, 0)$. In Table III, we represent $C_{2v}(y)$ for such symmetry. The table reveals that the point group of parity-mixed superconducting states may be either $C_{2v}(x)$, $C_{2v}(y)$, $C_{2v}(z)$ (anapole), or D_2 (monopole). We have shown the SCPE mode in the $C_{2v}(x)$ anapole and D_2 monopole states in Tables I and II, respectively. For completeness, we show the possible SCPE mode in the $C_{2v}(y)$ and $C_{2v}(z)$ anapole superconducting states in Tables IV and V, respectively.

We here comment on the derivation of the possible SCPE modes. Tables I, II, IV, and V are obtained by considering the condition that the supercurrent and strain belong to the same irreducible representation. An alternative way is to consider the compatible relation of irreducible representations. Because the SCPE tensor $d_{ijk}^{(SC)}$ becomes finite with the reduction of the symmetry of the system, $d_{ijk}^{(SC)}$ must belong to the totally symmetric representation in the superconducting state and not in the normal state. When we apply this condition to the D_{2h} point group, we find that finite SCPE coefficients $d_{ijk}^{(SC)}$ belong to the B_{3u} (A_u) irreducible representation in the $A_g + iB_{3u}$ anapole ($A_g + iA_u$ monopole) state.

APPENDIX B: ANALYSIS OF THE GROUP VELOCITY MODEL

In this Appendix, we show some notable properties of the group velocity model. First, we show the Bogoliubov spectrum in Fig. 14 assuming Cooper pairs' momentum $q_0 = 0$. The spectrum is asymmetric in the k_x direction and the asymmetry is reversed by changing the sign of the ASOC,

TABLE V. List of the IRs of the $C_{2v}(z)$ anapole superconducting state and corresponding strain s_{ij}, supercurrent J_k, and SCPE mode $d_{ijk}^{(SC)}$.

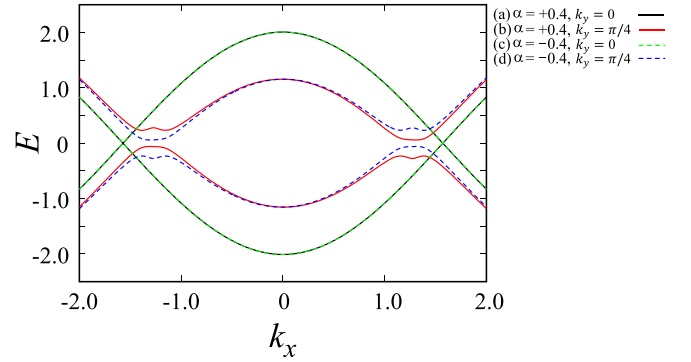| IR	Strain	Supercurrent	SCPE modes		
A_1	s_{xx}, s_{yy}, s_{zz}	J_z	$d_{xxz}^{(SC)}$	$d_{yyz}^{(SC)}$	$d_{zzz}^{(SC)}$
A_2	s_{xy}				
B_1	s_{yz}	J_y	$d_{yzy}^{(SC)}$		
B_2	s_{zx}	J_x	$d_{zxx}^{(SC)}$		

FIG. 14. The spectrum of Bogoliubov quasiparticles in the group velocity model for the $A_g + iB_{3u}$ anapole state. We show the energy dispersion along the k_x axis by setting $k_z = 0$ and [(a),(c)] $k_y = 0$ or [(b),(d)] $k_y = \pi/4$. The spectrum with $k_y = 0$ is gapless. [(a),(b)] The solid lines represent the spectrum calculated with $\alpha_x = 0.4$, while [(c),(d)] the dashed lines are obtained with $\alpha_x = -0.4$. We assume $\alpha_y = 0$, $\beta = 1$, $T = 0.01$, and set $q_0 = 0$.

α_x (see the spectrum for $k_y = \pi/4$). This property results in the α-antisymmetric behavior of the SCPE and q_0 in the group velocity model. Their β-antisymmetric behavior is also explained in the same way.

Next, we discuss the gap structure. Note that the spectrum is symmetric on the $k_y = 0$ and $k_y = \pi$ planes if we set $q_0 = 0$ (see Fig. 14 for $k_y = 0$). The analytic representation of the Bogoliubov spectrum on these planes is obtained as

$$E(\boldsymbol{k}) = \pm\sqrt{(\varepsilon_{\boldsymbol{k}} - \mu)^2 + \left(|\Delta_{\boldsymbol{k}}^+| \pm \beta\Delta_1 d_y^g\right)^2}, \quad \text{(B1)}$$

where $\Delta_{\boldsymbol{k}}^+ = \Delta_1 \psi^g + \Delta_2 d_z^u$. There are nodes in the superconducting gap when $\varepsilon_{\boldsymbol{k}} - \mu = 0$ and $|\Delta_{\boldsymbol{k}}^+| \pm \beta\Delta_1 d_y^g = 0$ are simultaneously satisfied on the planes. Indeed, for $\beta = 1$, the point node is present on the $k_y = 0$ plane, as we see in Fig. 14. When $\beta > 1$, Bogoliubov Fermi surfaces appear in several regions of the Brillouin zone. For instance, Fig. 15 shows the Bogoliubov spectrum indicating the Bogoliubov Fermi surface for $\beta = 1.01$. Thus, the superconducting gap
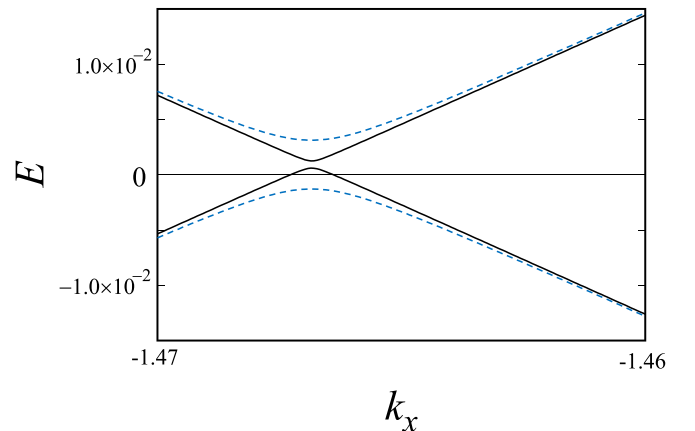

FIG. 15. The same plot as Fig. 14. The black solid (blue dashed) line shows the result for $\alpha_x = 0.4$ and $\beta = 1.01$ ($\beta = 1$). We set $k_y = -0.0481$ and $k_z = -0.457$ to show a part of the Bogoliubov Fermi surface.
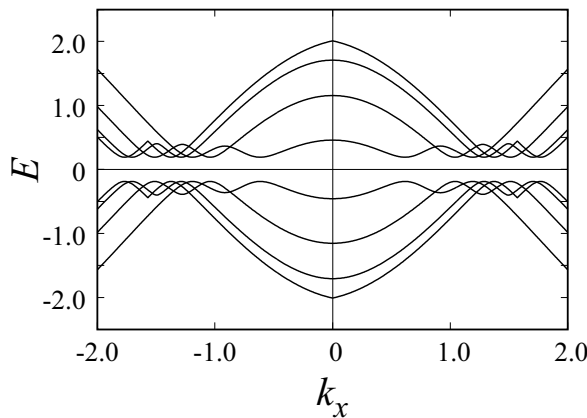
FIG. 16. The Bogoliubov spectrum of the $A_g + iB_{3u}$ state with $\alpha_x = -\alpha_y = 0.4$, $\beta = 0$ (geometric effect model), and $T = 0.01$. We draw the spectrum on $k_z = 0$ and $k_y = 0, \pi/8, \pi/4, 3\pi/8$.

structure significantly changes around $\beta = \pm 1$. This is the reason why the SCPE and q_0 show remarkable β dependence around $\beta = \pm 1$ in the group velocity model.

APPENDIX C: BOGOLIUBOV SPECTRUM IN THE GEOMETRIC EFFECT MODEL

Here, we show the energy spectrum of Bogoliubov quasiparticles in the geometric effect model. The spectrum without q_0 can be analytically calculated and obtained as

$$E(\mathbf{k}) = \pm \sqrt{(|g_{\mathbf{k}}^+| \pm \sqrt{(\varepsilon_{\mathbf{k}} - \mu)^2 + (\mathrm{Im}\Delta_{\mathbf{k}}^+)^2})^2 + (\mathrm{Re}\Delta_{\mathbf{k}}^+)^2},$$

(C1)

where $g_{\mathbf{k}}^+ = g_x + ig_y$. We confirm that the spectrum is symmetric for $\mathbf{k}$, i.e., $E(\mathbf{k}) = E(-\mathbf{k})$ in contrast to the group velocity model. In addition, since $\mathrm{Re}\Delta_{\mathbf{k}}^+ = \Delta_1 \psi^g > 0$ is always finite in our model, gap nodes are absent at least for $q_0 = 0$, Indeed, we see the gapped spectrum in Fig. 16.

[1] R. Wakatsuki, Y. Saito, S. Hoshino, Y. M. Itahashi, T. Ideue, M. Ezawa, Y. Iwasa, and N. Nagaosa, Sci. Adv. **3**, e1602390 (2017).

[2] R. Wakatsuki and N. Nagaosa, Phys. Rev. Lett. **121**, 026601 (2018).

[3] S. Hoshino, R. Wakatsuki, K. Hamamoto, and N. Nagaosa, Phys. Rev. B **98**, 054510 (2018).

[4] Y. M. Itahashi, T. Ideue, Y. Saito, S. Shimizu, T. Ouchi, T. Nojima, and Y. Iwasa, Sci. Adv. **6**, eaay9120 (2020).

[5] T. Schumann, L. Galletti, H. Jeong, K. Ahadi, W. M. Strickland, S. Salmani-Rezaie, and S. Stemmer, Phys. Rev. B **101**, 100503(R) (2020).

[6] S. Nakamura, K. Katsumi, H. Terai, and R. Shimano, Phys. Rev. Lett. **125**, 097004 (2020).

[7] Y. Miyasaka, R. Kawarazaki, H. Narita, F. Ando, Y. Ikeda, R. Hisatomi, A. Daido, Y. Shiota, T. Moriyama, Y. Yanase, and T. Ono, Appl. Phys. Express **14**, 073003 (2021).

[8] H. Watanabe, A. Daido, and Y. Yanase, Phys. Rev. B **105**, 024308 (2022).

[9] H. Watanabe, A. Daido, and Y. Yanase, Phys. Rev. B **105**, L100504 (2022).

[10] F. Ando, Y. Miyasaka, T. Li, J. Ishizuka, T. Arakawa, Y. Shiota, T. Moriyama, Y. Yanase, and T. Ono, Nature (London) **584**, 373 (2020).

[11] Y.-Y. Lyu, J. Jiang, Y.-L. Wang, Z.-L. Xiao, S. Dong, Q.-H. Chen, M. V. Milošević, H. Wang, R. Divan, J. E. Pearson, P. Wu, F. M. Peeters, and W.-K. Kwok, Nat. Commun. **12**, 2703 (2021).

[12] L. Bauriedl, C. Bäuml, L. Fuchs, C. Baumgartner, N. Paulik, J. M. Bauer, K.-Q. Lin, J. M. Lupton, T. Taniguchi, K. Watanabe *et al.*, Nat. Commun. **13**, 4266 (2022).

[13] C. Baumgartner, L. Fuchs, A. Costa, S. Reinhardt, S. Gronin, G. C. Gardner, T. Lindemann, M. J. Manfra, P. E. Faria Junior, D. Kochan *et al.*, Nat. Nanotechnol. **17**, 39 (2022).

[14] H. Wu, Y. Wang, Y. Xu, P. K. Sivakumar, C. Pasco, U. Filippozzi, S. S. P. Parkin, Y.-J. Zeng, T. McQueen, and M. N. Ali, Nature (London) **604**, 653 (2022).

[15] H. Narita, J. Ishizuka, R. Kawarazaki, D. Kan, Y. Shiota, T. Moriyama, Y. Shimakawa, A. V. Ognev, A. S. Samardak, Y. Yanase, and T. Ono, Nat. Nanotechnol. **17**, 823 (2022).

[16] J.-X. Lin, P. Siriviboon, H. D. Scammell, S. Liu, D. Rhodes, K. Watanabe, T. Taniguchi, J. Hone, M. S. Scheurer, and J. I. A. Li, Nat. Phys. **18**, 1221 (2022).

[17] A. A. Kopasov, A. G. Kutlin, and A. S. Mel'nikov, Phys. Rev. B **103**, 144520 (2021).

[18] N. F. Q. Yuan and L. Fu, Proc. Natl. Acad. Sci. USA **119**, e2119548119 (2022).

[19] A. Daido, Y. Ikeda, and Y. Yanase, Phys. Rev. Lett. **128**, 037001 (2022).

[20] J. J. He, Y. Tanaka, and N. Nagaosa, New J. Phys. **24**, 053014 (2022).

[21] S. Ilić and F. S. Bergeret, Phys. Rev. Lett. **128**, 177001 (2022).

[22] H. F. Legg, D. Loss, and J. Klinovaja, Phys. Rev. B **106**, 104501 (2022).

[23] H. D. Scammell, J. I. A. Li, and M. S. Scheurer, 2D Mater. **9**, 025027 (2022).

[24] J. Jiang, M. V. Milošević, Y.-L. Wang, Z.-L. Xiao, F. M. Peeters, and Q.-H. Chen, Phys. Rev. Appl. **18**, 034064 (2022).

[25] A. Daido and Y. Yanase, Phys. Rev. B **106**, 205206 (2022).

[26] R. Kawarazaki, H. Narita, Y. Miyasaka, Y. Ikeda, R. Hisatomi, A. Daido, Y. Shiota, T. Moriyama, Y. Yanase, A. V. Ognev, A. S. Samardak, and T. Ono, Appl. Phys. Express **15**, 113001 (2022).

[27] J. Ishizuka and Y. Yanase, Phys. Rev. B **103**, 094504 (2021).

[28] S. Ran, I.-L. Liu, Y. S. Eo, D. J. Campbell, P. M. Neves, W. T. Fuhrman, S. R. Saha, C. Eckberg, H. Kim, D. Graf *et al.*, Nat. Phys. **15**, 1250 (2019).

[29] D. Braithwaite, M. Vališka, G. Knebel, G. Lapertot, J.-P. Brison, A. Pourret, M. E. Zhitomirsky, J. Flouquet, F. Honda, and D. Aoki, Commun. Phys. **2**, 147 (2019).

[30] D. Aoki, F. Honda, G. Knebel, D. Braithwaite, A. Nakamura, D. Li, Y. Homma, Y. Shimizu, Y. J. Sato, J.-P. Brison, and J. Flouquet, J. Phys. Soc. Jpn. **89**, 053705 (2020).

[31] D. Aoki, J.-P. Brison, J. Flouquet, K. Ishida, G. Knebel, Y. Tokunaga, and Y. Yanase, J. Phys.: Condens. Matter **34**, 243002 (2022).

[32] A. Rosuel, C. Marcenat, G. Knebel, T. Klein, A. Pourret, N. Marquardt, Q. Niu, S. Rousseau, A. Demuer, G. Seyfarth, G. Lapertot, D. Aoki, D. Braithwaite, J. Flouquet, and J. P. Brison, Phys. Rev. X **13**, 011022 (2023).

[33] K. Kinjo, H. Fujibayashi, S. Kitagawa, K. Ishida, Y. Tokunaga, H. Sakai, S. Kambe, A. Nakamura, Y. Shimizu, Y. Homma, D. X. Li, F. Honda, D. Aoki, K. Hiraki, M. Kimata, and T. Sasaki, Phys. Rev. B **107**, L060502 (2023).

[34] H. Sakai, Y. Tokiwa, P. Opletal, M. Kimata, S. Awaji, T. Sasaki, D. Aoki, S. Kambe, Y. Tokunaga, and Y. Haga, Phys. Rev. Lett. **130**, 196002 (2023).

[35] Y. Wang and L. Fu, Phys. Rev. Lett. **119**, 187003 (2017).

[36] H. Watanabe and Y. Yanase, Phys. Rev. B **96**, 064432 (2017).

[37] S. Kanasugi and Y. Yanase, Commun. Phys. **5**, 39 (2022).

[38] T. Kitamura, S. Kanasugi, M. Chazono, and Y. Yanase, Phys. Rev. B **107**, 214513 (2023).

[39] P. Fulde and R. A. Ferrell, Phys. Rev. **135**, A550 (1964).

[40] A. I. Larkin and Y. N. Ovchinnikov, Zh. Eksp. Teor. Fiz. **47**, 1136 (1964).

[41] E. Bauer and M. Sigrist, *Non-Centrosymmetric Superconductors: Introduction and Overview* (Springer, Heidelberg, 2012).

[42] M. Smidman, M. B. Salamon, H. Q. Yuan, and D. F. Agterberg, Rep. Prog. Phys. **80**, 036501 (2017).

[43] M. Chazono, H. Watanabe, and Y. Yanase, Phys. Rev. B **105**, 024509 (2022).

[44] M. H. Fischer, M. Sigrist, D. F. Agterberg, and Y. Yanase, Annu. Rev. Condens. Matter Phys. **14**, 153 (2023).

[45] H. Watanabe and Y. Yanase, Phys. Rev. B **98**, 245129 (2018).

[46] N. Marzari and D. Vanderbilt, Phys. Rev. B **56**, 12847 (1997).

[47] R. Resta, Eur. Phys. J. B **79**, 121 (2011).

[48] S. Peotta and P. Törmä, Nat. Commun. **6**, 8944 (2015).

[49] L. Liang, T. I. Vanhala, S. Peotta, T. Siro, A. Harju, and P. Törmä, Phys. Rev. B **95**, 024515 (2017).

[50] P. Törmä, S. Peotta, and B. A. Bernevig, Nat. Rev. Phys. **4**, 528 (2022).

[51] Y. Gao, S. A. Yang, and Q. Niu, Phys. Rev. Lett. **112**, 166601 (2014).

[52] Y. Gao and D. Xiao, Phys. Rev. Lett. **122**, 227402 (2019).

[53] M. F. Lapa and T. L. Hughes, Phys. Rev. B **99**, 121111(R) (2019).

[54] A. Daido, A. Shitade, and Y. Yanase, Phys. Rev. B **102**, 235149 (2020).

[55] A. Julku, G. M. Bruun, and P. Törmä, Phys. Rev. B **104**, 144507 (2021).

[56] A. Julku, G. M. Bruun, and P. Törmä, Phys. Rev. Lett. **127**, 170404 (2021).

[57] J. Ahn, G.-Y. Guo, and N. Nagaosa, Phys. Rev. X **10**, 041041 (2020).

[58] H. Watanabe and Y. Yanase, Phys. Rev. X **11**, 011001 (2021).

[59] J.-W. Rhim, K. Kim, and B.-J. Yang, Nature (London) **584**, 59 (2020).

[60] D. D. Solnyshkov, C. Leblanc, L. Bessonart, A. Nalitov, J. Ren, Q. Liao, F. Li, and G. Malpuech, Phys. Rev. B **103**, 125302 (2021).

[61] Q. Liao, C. Leblanc, J. Ren, F. Li, Y. Li, D. Solnyshkov, G. Malpuech, J. Yao, and H. Fu, Phys. Rev. Lett. **127**, 107402 (2021).

[62] Y. Shiomi, H. Watanabe, H. Masuda, H. Takahashi, Y. Yanase, and S. Ishiwata, Phys. Rev. Lett. **122**, 127207 (2019).

[63] Y. Shiomi, H. Masuda, H. Takahashi, and S. Ishiwata, Sci. Rep. **10**, 7574 (2020).

[64] D. F. Agterberg, P. M. R. Brydon, and C. Timm, Phys. Rev. Lett. **118**, 127001 (2017).

[65] P. M. R. Brydon, D. F. Agterberg, H. Menke, and C. Timm, Phys. Rev. B **98**, 224509 (2018).

[66] J. M. Link and I. F. Herbut, Phys. Rev. Lett. **125**, 237004 (2020).

[67] S. Autti, J. T. Mäkinen, J. Rysti, G. E. Volovik, V. V. Zavjalov, and V. B. Eltsov, Phys. Rev. Res. **2**, 033013 (2020).

[68] C. Setty, Y. Cao, A. Kreisel, S. Bhattacharyya, and P. J. Hirschfeld, Phys. Rev. B **102**, 064504 (2020).

[69] J. Ahn and N. Nagaosa, Nat. Commun. **12**, 1617 (2021).

[70] K. Ushida, T. Yanagisawa, R. Hibino, M. Matsuda, H. Hidaka, H. Amitsuka, G. Knebel, J. Flouquet, and D. Aoki, arXiv:2211.08354.